Nano Energy 102 (2022) 107641

Contents lists available at ScienceDirect

Nano Energy

journal homepage: www.elsevier.com/locate/nanoen

Lithium metal stripping mechanisms revealed through electrochemical liquid cell electron microscopy

Seung-Yong Lee [a,b,c], Junyi Shangguan [a,d], Sophia Betzler [a], Stephen J. Harris [e], Marca M. Doeff [e], Haimei Zheng [a,d,*]

[a] *Materials Sciences Division, Lawrence Berkeley National Laboratory, Berkeley, CA, USA*
[b] *Division of Materials Science and Engineering, Hanyang University, Seoul, Republic of Korea*
[c] *Department of Chemical Engineering, Hanyang University, Seoul, Republic of Korea*
[d] *Department of Material Science and Engineering, University of California, Berkeley, CA, USA*
[e] *Energy Storage and Distributed Resources Division, Lawrence Berkeley National Laboratory, Berkeley, CA, USA*

A R T I C L E I N F O

Keywords:
Electrochemical liquid cell transmission electron microscopy
Lithium-ion battery
Lithium metal anode
Lithium stripping
Solid-electrolyte interphase

A B S T R A C T

An understanding of lithium stripping is as important as that of lithium plating to achieve significant advances in using lithium metal anodes for high-energy rechargeable batteries. However, there have been limited studies on lithium stripping compared to lithium plating. Here we report the lithium stripping mechanisms revealed through *in-situ* electrochemical liquid cell transmission electron microscopy (TEM). We directly observe and compare the stripping behavior of the *in-situ* grown lithium dendrites and lithium nanograins covered by a lithium fluoride-rich solid-electrolyte interphase (SEI). We find the sporadic lithium stripping behavior and three important modes that can describe the stripping of individual lithium deposits, regardless of their morphology: (i) symmetric stripping, (ii) surface-preferred asymmetric stripping, and (iii) interface-preferred asymmetric stripping. In addition, SEI chemical mapping with high spatial resolution shows a remarkable SEI loss at the end of the lithium metal stripping, which illustrates the importance of SEI protection in the subsequent cycles.

1. Introduction

Increasing demands for energy storage devices with much higher energy density have attracted a revival of interest in lithium metal anodes for future rechargeable batteries [1,2]. However, it remains a great challenge to use lithium metal as an anode because of safety issues associated with lithium dendrite formation, which may result in short-circuiting of the batteries [3]. In addition, the formation of "dead lithium" during the stripping cycles, which refers to fragmentation of lithium deposits detached from the electrode, may also result in capacity loss [4–6]. These challenges have led to much research effort aimed at understanding and controlling lithium dendrite growth [3,7]. For example, the formation of large lithium dendrites under a polymer electrolyte has been observed using x-ray techniques [8]. Moreover, the atomic structures of lithium dendrites and solid-electrolyte interphase (SEI) have been revealed by cryogenic electron microscopy [9,10]. Recently, with *in-situ* electrochemical liquid cell transmission electron microscopy (TEM), lithium nanogranules instead of lithium dendrites were obtained through modifying the SEI composition by applying a thin cationic polymer film on the electrode [11]. Extensive studies have shown that SEI on lithium metal deposits plays a key role in transforming the lithium growth behavior [12–14]. In contrast, there have been limited studies on the stripping mechanisms of lithium, even though it is as important as lithium plating for improving the performance of lithium metal batteries [15–21]. For example, fast accumulation of voids under high stripping rates [16], different lithium plating/stripping behaviors from initially plated and stripped lithium electrode [17], and critical stripping current density causing lithium dendrite formation during the following cycle [18] were investigated at microscales by scanning electron microscopy studies. Previous studies suggested potential models of dead lithium formation, however, the limited spatial resolution hinders the in-depth understanding of lithium stripping mechanisms and the relevant dead lithium formation. In addition, although an elaborate *in-situ* optical microscopy showed intact SEI after the lithium stripping [19], providing a very rare study on lithium SEI, technical advances allowing further quantitative interpretations of SEI behaviors during the lithium stripping are needed.

Here, we investigate lithium stripping behavior using a state-of-the-

* Corresponding author at: Materials Sciences Division, Lawrence Berkeley National Laboratory, Berkeley, CA, USA.
E-mail address: hmzheng@lbl.gov (H. Zheng).

https://doi.org/10.1016/j.nanoen.2022.107641
Received 1 June 2022; Received in revised form 22 July 2022; Accepted 26 July 2022
Available online 28 July 2022

art *in-situ* electrochemical liquid cell TEM [22]. The *in-situ* liquid cell TEM allows direct observation of the electrochemical plating/stripping processes of lithium metal in a common liquid electrolyte for lithium ion batteries. We compare the stripping process of lithium dendrites and lithium nanogranular deposits. We focus in particular on dead lithium formation during lithium stripping. By correlating the lithium morphology evolution during stripping with the chemistry of SEI, lithium stripping mechanisms are elucidated.

2. Results and discussion

2.1. Electrochemical liquid cell TEM experiments for lithium stripping studies

The experimental setup of the electrochemical liquid cell TEM for *in-situ* lithium plating/stripping is shown in Fig. 1a-c. A liquid electrolyte (1M $LiPF_6$ in propylene carbonate (PC)) was filled in a Si/SiN_x electrochemical nano-cell where titanium was deposited as current collectors for the working/counter electrodes (Fig. 1a) [23]. Lithium flakes were attached on the rear side of the both Ti electrodes to allow reversible electrochemical reactions and supply lithium ions in case there is no source at the front lines. Experimental details are described further in the *Material and methods* section. Potential electron beam effects during the *in-situ* lithium plating/stripping experiments were comprehensively investigated and elaborated in Supplementary Material (Supplementary Note 1 and Figure S1). We studied stripping behaviors of lithium deposits grown *in-situ* in the electrochemical liquid cells with dendritic or nanogranular structures, as shown in Fig. 1b and c. The different morphologies of the lithium deposits were achieved by modifying the electrode environment with a poly(diallyldimethylammonium chloride) (PDDA) cationic polymer film coating. As elaborated in our previous study [11], by applying a thin layer of the PDDA cationic polymer film on the electrode, PF_6^- salt anions are attracted to the electrode surface by electrostatic force, promoting the formation of a lithium fluoride (LiF)-rich SEI on the lithium deposits. The LiF-rich SEI inhibits dendritic growth of lithium, resulting in lithium nanogranular growth instead [24, 25]. The LiF-rich SEI on lithium nanogranules can be identified in the annular dark-field (ADF) scanning TEM (STEM) images and

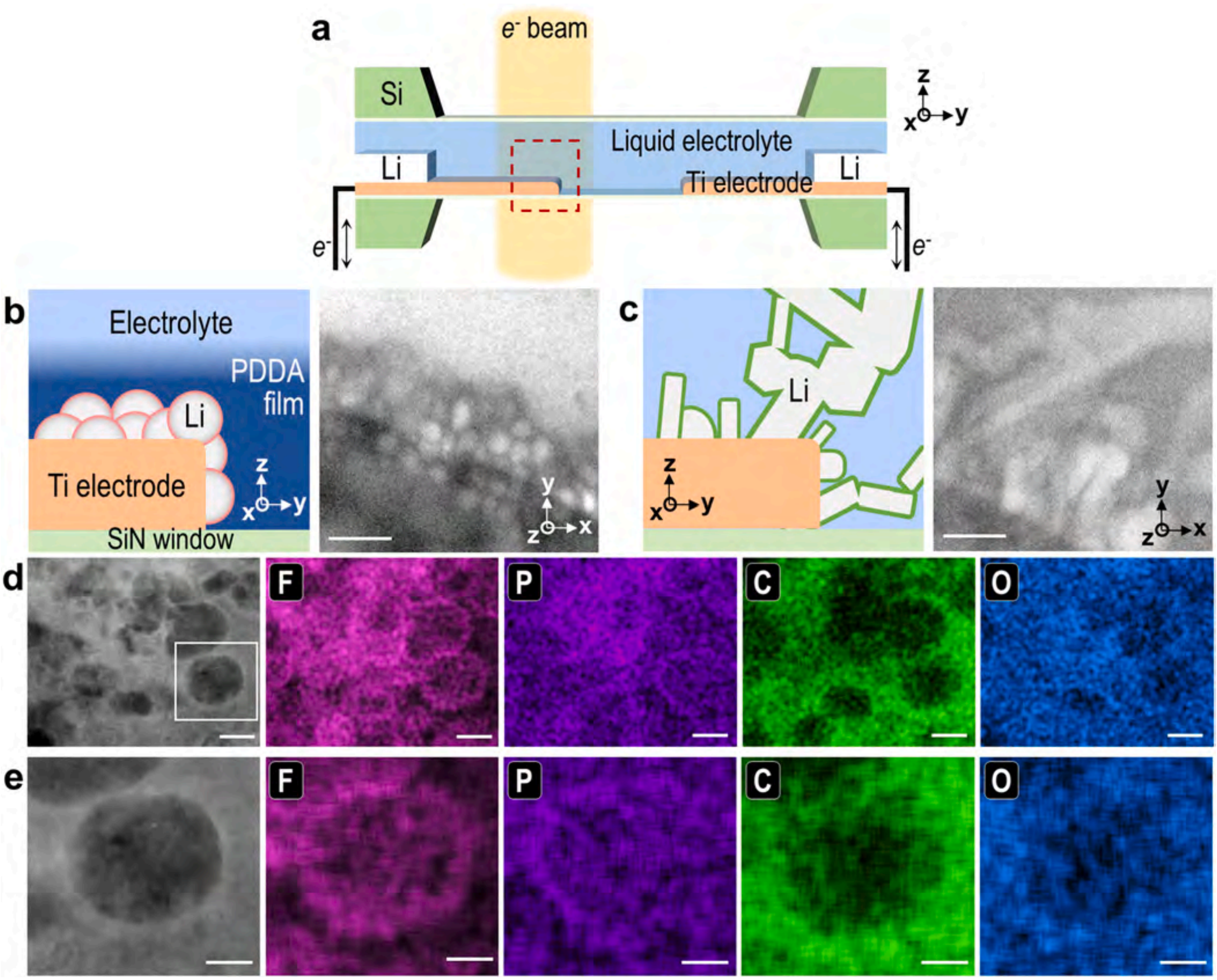

Fig. 1. Schematic drawings of electrochemical liquid cell transmission electron microscopy (TEM) experimental designs for Li stripping studies and chemical images of *in-situ* grown lithium deposits with LiF-rich solid-electrolyte interphase (SEI). (a) A schematic drawing of an electrochemical liquid cell for *in-situ* TEM lithium plating/stripping experiments. (b, c) Illustrations (left panels) and TEM images (right panels) of the *in-situ* grown (b) lithium nanogranules with LiF-rich SEI and (c) lithium dendrites at the area corresponding to the red square in (a). Scale bars are 500 nm. (d) An annular dark-field (ADF) scanning TEM (STEM) image and energy-dispersive x-ray spectroscopy (EDS) elemental maps of lithium nanogranules with LiF-rich SEI. Scale bars are 200 nm. (e) A magnified ADF-STEM image and EDS elemental maps of a lithium nanogranule marked in (d). Scale bars are 100 nm.

corresponding energy dispersive x-ray spectroscopy (EDS) elemental maps (Fig. 1d and e). An additional ADF-STEM image and EDS elemental maps at lower magnification are provided in Supplementary Material (Figure S2) for better understanding of the experimental results. The ADF-STEM image in Fig. 1d shows a cluster of lithium nanogranules. The darker contrast of the nanogranules is due to the low atomic number of lithium, resulting in lower scattering angles of the incident electrons compared to those from other elements, *e.g.* carbon, oxygen, fluorine, phosphorus, *etc* [26]. In the EDS maps, both of fluorine and phosphorus are concentrated on the surface of lithium nanogranules but fluorine is covered much more uniformly than phosphorus. Carbon and oxygen are broadly distributed in the outer layer of SEI and the residual electrolyte around the lithium nanogranules. The LiF-rich SEI on lithium nanogranules compared with lithium dendrites was confirmed by x-ray photoelectron spectroscopy (XPS), as shown in our recent publication [11].

2.2. *Stripping modes of individual LiF SEI-rich lithium nanogranules*

Supplementary material related to this article can be found online at doi:10.1016/j.nanoen.2022.107641.

TEM images of lithium nanogranules with LiF-rich SEI on the Ti electrode before and after the *in-situ* lithium stripping are shown in Fig. 2a and b (also see Video S1). The TEM images show part of the Ti electrode viewed from above with lithium metal deposits, bright contrasts in the bright-field TEM images, laying on top of the Ti electrode. The black nanowires and nanoparticles are $Sn@SnO_2$ nanostructures, which were used to assist PDDA cationic polymer coating in the electrochemical liquid cell [11]. The $Sn@SnO_2$ nanostructures did not contribute to the electrochemical reactions, probably due to their high contact resistance in the electrochemical liquid cell, which can be confirmed by the fact that their volume did not change [11]. Most lithium nanogranules on the electrode were stripped after applying a positive electric potential for a period of time, as shown in Fig. 2a and b. Control experiments ruled out potential effects of the electron beam on the lithium stripping (Figure S1). Different stripping behaviors were observed for individual lithium nanogranules grown simultaneously under the same experimental condition as shown in Fig. 2c-j.

We found three stripping modes of individual lithium nanogranules (Fig. 2c): (i) symmetric stripping (Li I, II; Fig. 2d-f), (ii) surface-preferred asymmetric stripping (Li III; Fig. 2g,h), and (iii) interface-preferred asymmetric stripping (Li IV; Fig. 2i,j). A number of factors may have contributed to the observed different stripping behaviors of lithium nanogranules, such as variations in the local SEI conditions, different morphology of lithium deposits, local inhomogeneity of the surrounding electrolyte, the status of electrical contact, *etc.* In the symmetric

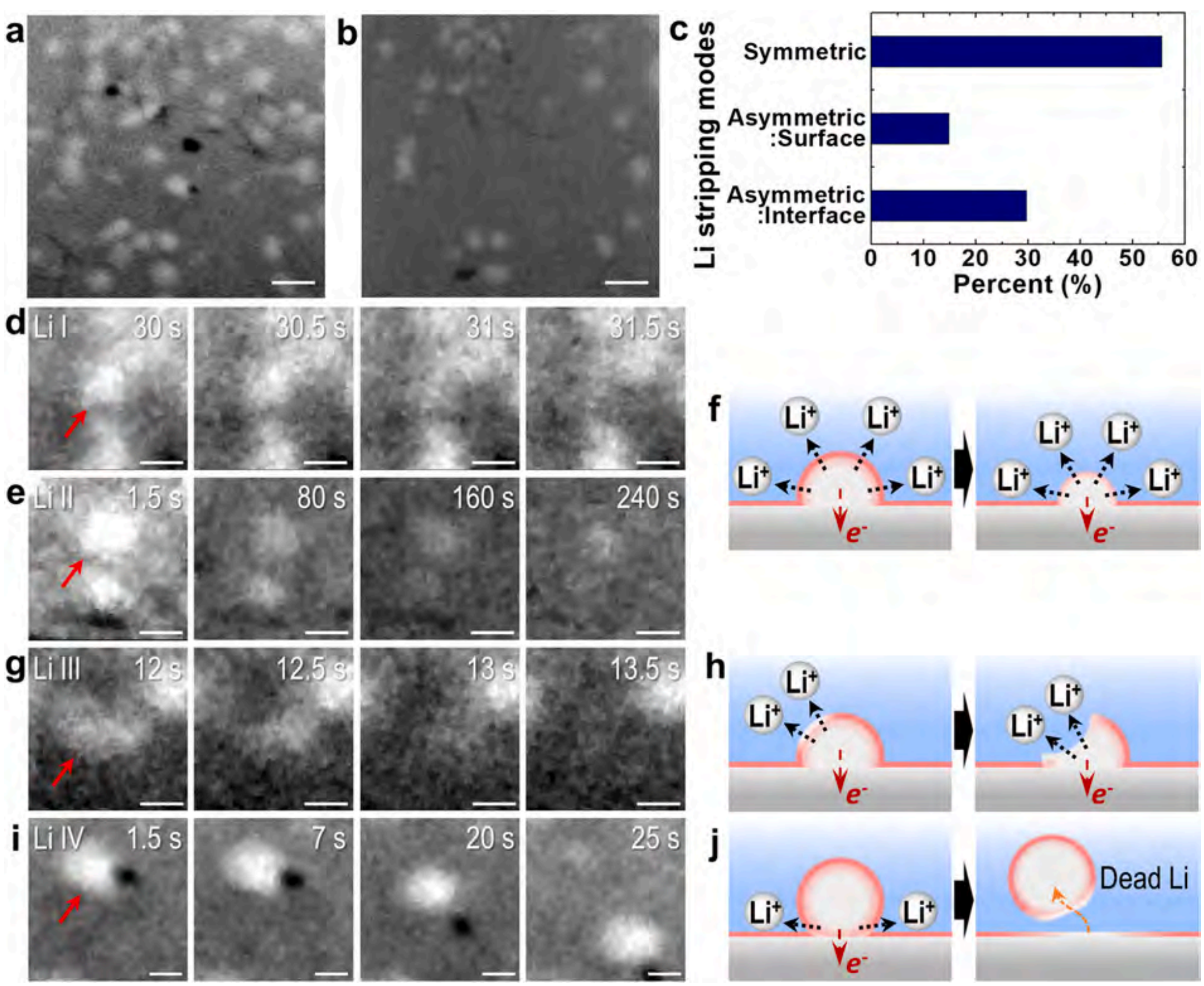

Fig. 2. Stripping modes of lithium nanogranules on top of the titanium electrode with LiF-rich SEI. (a, b) TEM images of the electrode area captured (a) before and (b) after the *in-situ* lithium stripping (Video S1). The images are a top view of a portion of the Ti electrode. Scale bars are 500 nm. (c) Relative frequency distribution of each stripping mode for lithium nanogranules with LiF-rich SEI. (d, e, g, i) Sequential TEM images of *in-situ* stripping and (f, h, j) corresponding schematic illustrations of lithium stripping modes: (d, e, f) symmetric (Video S2 and S3), (g, h) surface-preferred asymmetric (Video S4), and (i, j) interface-preferred asymmetric stripping modes (Video S5). Scale bars are 200 nm.

stripping mode, the lithium nanogranule shrinks inward radially, preserving its round shape. The corresponding uniform decreases of size and contrast are clearly visible in Fig. 2d and e (also see Video S2 and S3). In contrast to the symmetric lithium stripping, surface-preferred asymmetric stripping is defined as the case that the stripping starts from a certain side position at the surface of lithium nanogranule. Fig. 2g shows an example of this surface-preferred asymmetric stripping mode (also see Video S4). The upper-left corner of the lithium nanogranule is first stripped at 12.5 s. Interestingly, stripping continues rapidly from a neighboring position (at 13 s, Fig. 2g). This shows that the collapsed SEI layer at the lithium-stripped position may ease further lithium stripping through that position (Fig. 2h). The surface-preferred asymmetric stripping mode was not frequently observed (Fig. 2c), which shows that most of the lithium nanogranules were in a fairly homogeneous environment. We also note that lithium stripping triggered at specific points does not always lead to the rapid complete stripping of lithium deposits, as partially stripped lithium nanogranules were observed after the *in-situ* stripping as shown in Figure S3. The interface-preferred asymmetric stripping mode refers to preferential lithium stripping at the interface between the lithium deposit and the electrode (current collector), which contributes significantly to "dead lithium" formation. Fig. 2i shows an example of the interface-preferred asymmetric stripping mode (also see Video S5). After several seconds of stripping, the lithium nanogranule marked in Fig. 2i became dead lithium floating in the liquid electrolyte. This indicates preferential lithium stripping at the Li/electrode interface resulting in the separation of the lithium deposit from the electrode (Fig. 2j), which is distinct from coincidental desorption of lithium nanogranules from the electrode as further described in Supplementary Material. It could be influenced by a higher energy of the electrolyte-lithium-electrode triple point than that of other surface points, which might explain why there are twice as many interface stripping events as surface stripping events (Fig. 2c). It shows a drawback of tiny lithium deposits (*e.g.* nanogranules) with small contact areas to the electrode, which leads to higher chance of losing the electrical connection during their stripping, resulting in the dead lithium formation.

Stripping rates of individual lithium nanogranules are compared in Fig. 3. Area changes of the individual lithium nanogranules shown in Fig. 2d (Li I; symmetric stripping), Fig. 2e (Li II; symmetric stripping), Fig. 2g (Li III; surface-preferred asymmetric stripping), and Fig. 2i (Li IV; interface-preferred asymmetric stripping) were tracked as a function of time. The measurement details are further discussed in Supplementary Material. The plot shows that the stripping kinetics of individual lithium deposits, including reaction initiation time and reaction speed, are heavily influenced by local environments. Mostly, lithium nanogranules were stripped very rapidly following the initiation, as shown in cases of Li I and Li III. The stripping reactions were completed within several seconds. However, some lithium nanogranules had a considerably slower stripping rate. As shown in cases of Li I and Li II, there is a significant difference of the lithium stripping rate even in the same stripping mode. Note that the plot for Li IV shows there was almost no area change of Li IV before it lost the contact with the electrode and became the dead lithium.

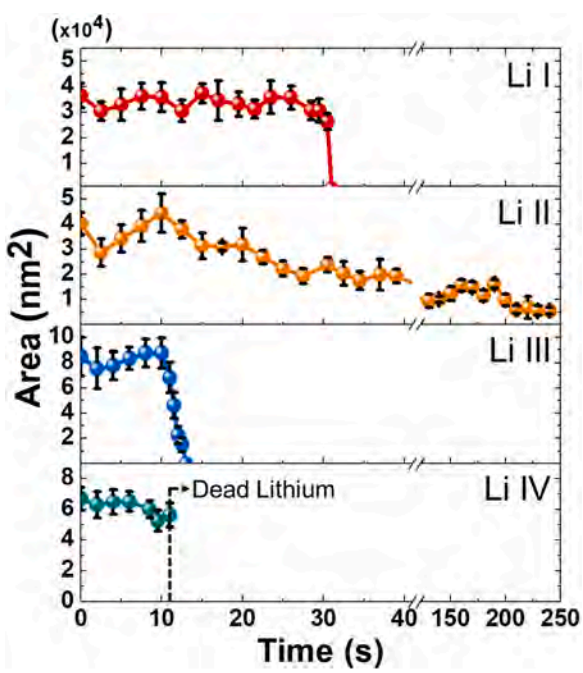

Fig. 3. A comparison of lithium nanogranule stripping rates. Size reduction of individual lithium nanogranules labeled as Li I (Fig. 2d; symmetric stripping), Li II (Fig. 2e; symmetric stripping), Li III (Fig. 2g; surface-preferred asymmetric stripping) and Li IV (Fig. 2i; interface-preferred asymmetric stripping).

2.3. Sporadic stripping behavior of lithium metal deposits

We also found an interesting overall lithium stripping behavior; neighboring lithium deposits are stripped sporadically rather than simultaneously. In other words, lithium deposits in immediate proximity to the rapidly stripped lithium deposit are not stripped immediately. This behavior is shown in Fig. 4a. The numbers labeled on the TEM image indicate the stripping sequence of individual lithium nanogranules in about 10 μm^2 area. The start and finish times of each stripping event for different lithium nanogranules are shown in Table 1. TEM images before and after each stripping event are shown in Figure S5. The labeled lithium deposits were stripped rapidly, but their neighboring ones were not stripped immediately, which was generally observed regardless of the symmetric or asymmetric stripping behavior of individual lithium deposits (Video S1). We propose that the rapid stripping of one lithium deposit impedes stripping of adjacent deposits by increasing the local concentration of lithium ions. The lithium ion concentration changes as a result of a single lithium deposit stripping are shown in Fig. 4b and c. These were calculated using Eq. (1), assuming that the rapidly stripped lithium deposit is an instantaneous point source for the lithium-ion diffusion [27].

$$C(x, y, t) = \frac{M}{4\pi D L_z t} e^{-\frac{x^2+y^2}{4Dt}} + C_0 \quad (1)$$

In Eq. (1), $C(x, y, t)$ refers to the Li^+ concentration of position (x, y) at time t, M is total mol number of the Li^+ point source, D is the Li^+ diffusion coefficient, L_z is the thickness of the liquid cell compensating the missing dimension, and C_0 is the base Li^+ concentration from the electrolyte. The calculation details are described further in Supplementary Material. As shown in Fig. 4b, stripping of a lithium deposit causes instantaneous great increases of Li^+ concentration in its neighborhood. Fig. 4c shows that the Li^+ concentration at positions about 500 nm away can be doubled within 0.5 ms after the stripping of the lithium deposit. This increased local Li^+ concentration may increase the potential required for the stripping of these adjacent lithium deposits and slow down their dissolution rates momentarily, facilitating the stripping of lithium deposits elsewhere.

2.4. Stripping modes of individual lithium dendrites

Supplementary material related to this article can be found online at doi:10.1016/j.nanoen.2022.107641.

We also investigated stripping behaviors of typical lithium dendrites and found that the stripping behaviors of lithium dendrites share many similarities with those of lithium nanogranules. Fig. 5a and b show TEM images of the lithium dendrites before and after the *in-situ* stripping experiment. The lithium dendrites were *in-situ* plated and stripped under the same experimental conditions as those for the lithium nanogranular growth but in the absence of the polymer film coating. Detailed stripping

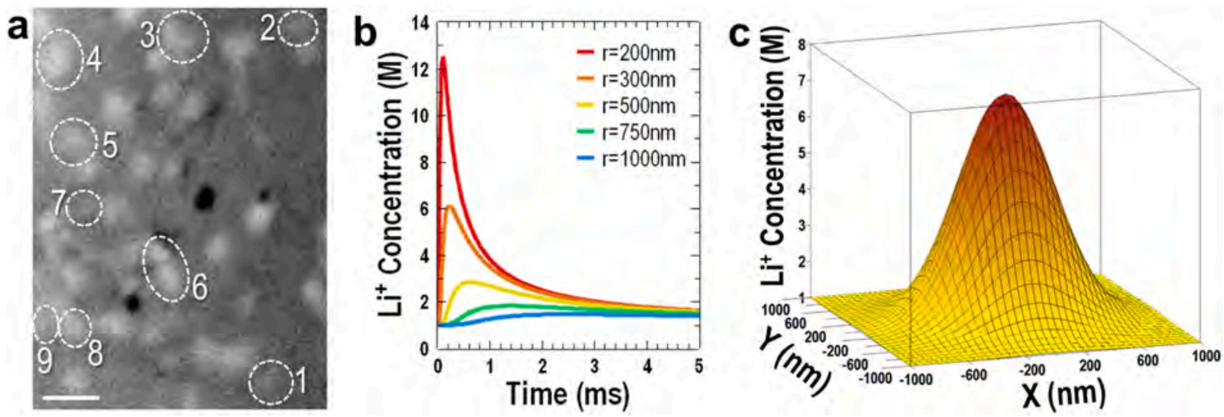

Fig. 4. Spatially scattered stripping behavior of lithium deposits. (a) A TEM image marked with the stripping sequence of lithium nanogranules and their positions. The image is a top view of a portion of the Ti electrode. Scale bar is 500 nm. (b, c) Estimation of surrounding Li-ion concentration changes as a result of a single lithium deposit stripping. (b) Calculations of Li-ion concentration changes with time at certain distances (denoted as "r") from a stripped lithium deposit. (c) Calculations of Li-ion concentration distribution around a lithium deposit after 0.5 ms of its stripping.

Table 1
Stripping start and end times of individual lithium nanogranules labeled on a TEM image in Fig. 4a.

Li deposit	Stripping start time [s]	Stripping end time [s]
1	4.0	6.0
2	5.5	7.0
3	7.5	9.5
4	11.5	13.0
5	17.0	18.0
6	21.0	22.5
7	25.0	25.5
8	30.0	31.0
9	37.5	38.0

modes of lithium dendrites are shown in Fig. 5c-f. We found that the stripping modes of lithium dendrites follow those of lithium nanogranules. Fig. 5c shows the stripping of a short lithium dendrite with a length of 700 nm and a width of 400 nm. We note that rapid lithium self-discharge contributed to the stripping of the lithium deposit from stage (I) to (II) in Fig. 5c, as further discussed in the Supplementary Material (Figure S6). The small lithium deposit was stripped preferentially from the left side by the surface-preferred asymmetric stripping mode. The lithium deposit was fully stripped within one second during the *in-situ* lithium stripping (see Video S7). This shows that short and straight lithium deposits can be stripped easily even under the asymmetric stripping mode, as shown in Fig. 5d. However, majority of lithium deposits have long branched dendrite structures, which preferentially separate at branch-branch interface during the stripping. This causes significant dead lithium formation. This asymmetric stripping of the branched dendrite is displayed in Fig. 5e. This might have originated from the SEI inhomogeneity at the Li/Li interface that can lead to the easier lithium-ion extraction at this position. Or, it could be due to the higher energy of the interface compared to other positions, which eases the charge transfer reaction. This stripping process is schematically illustrated in Fig. 5f. It clearly shows a critical origin of dead lithium formation from lithium dendrites, which had not been demonstrated before.

2.5. Impact of lithium stripping on SEI layer

We further trace the impact of lithium stripping on SEI layer. This is essential to determine whether the SEI formed in the previous cycle can be beneficial for the following cycle. With the stripping of lithium nanogranules as an example, SEIs on the electrodes before and after stripping were measured using STEM-EDS. The EDS fluorine maps before and after the stripping of lithium nanogranules are shown in Fig. 6 and additional EDS elemental maps are shown in Figure S7. Fig. 6a-c shows *in-situ* plated lithium nanogranules and corresponding EDS fluorine map. Consistent with the EDS elemental maps in Fig. 1d, fluorine-rich SEI is clearly visible for individual lithium nanogranules (Fig. 6c). There is an obvious concentration difference of fluorine between areas with and without lithium nanogranules. Fig. 6d and e show TEM images obtained before and after the *in-situ* lithium stripping experiments. Most lithium nanogranules were stripped leaving only small remains and traces behind, shown as dark contrast at the corresponding positions in the ADF-STEM image (Fig. 6f). Interestingly, the fluorine concentration differs between areas with and without the remaining lithium nanogranule after the stripping (Fig. 6g).

The SEI concentration ratio before and after lithium stripping were quantitatively compared by EDS spectra collected from different electrode areas: (i) densely covered by plated lithium nanogranules (Area 1 in Fig. 6c), (ii) free from lithium after the lithium plating experiment (Area 2 in Fig. 6c), and (iii) after lithium stripping (Area 3 in Fig. 6g). Fig. 6h shows the relative atomic ratios of representative elements of the SEI, *i.e.* fluorine (n_F/n_{Ti}), phosphorus (n_P/n_{Ti}), and oxygen (n_O/n_{Ti}), scaled relative to titanium for the electrode as reference. For example, in Area 1, the concentration of fluorine is equivalent to 76 % of Ti concentration. As titanium electrode is uniformly deposited on the bottom chip of each liquid cell and it is electrochemically inactive during the *in-situ* experiment, the EDS signal of titanium concurrently measured at each area can be a good reference for the quantitative comparison. There is little difference on the amount of phosphorus and oxygen at all areas, however, the fluorine concentration significantly decreased on the electrode after the lithium stripping (Area 1 *vs.* 3). The fluorine amount after the lithium stripping (Area 3) is comparable to that of the electrode area where lithium was not deposited during the lithium plating experiment (Area 2). This indicates that the collapsed SEI layers (mostly LiF in this case) drift away in the electrolyte during lithium stripping. These results suggest that "good SEI" formed during the prior lithium plating step will be hardly beneficial to the next cycle unless it is tightly fastened by other supporting materials. The SEI behavior during lithium stripping is schematically drawn in Fig. 6i. Our discovery of the substantial SEI loss, possibly during every cycle, provides valuable information for the future development of lithium metal batteries. LiF within SEI has been known to be promising for lithium dendrite suppression and the high Li/LiF interfacial energy is considered an important factor [28]. However, the high interfacial energy can also lead to small spherical lithium deposits with excess SEI rendering them sensitive to SEI loss every cycle. This illustrates that LiF-rich SEI conditions must be

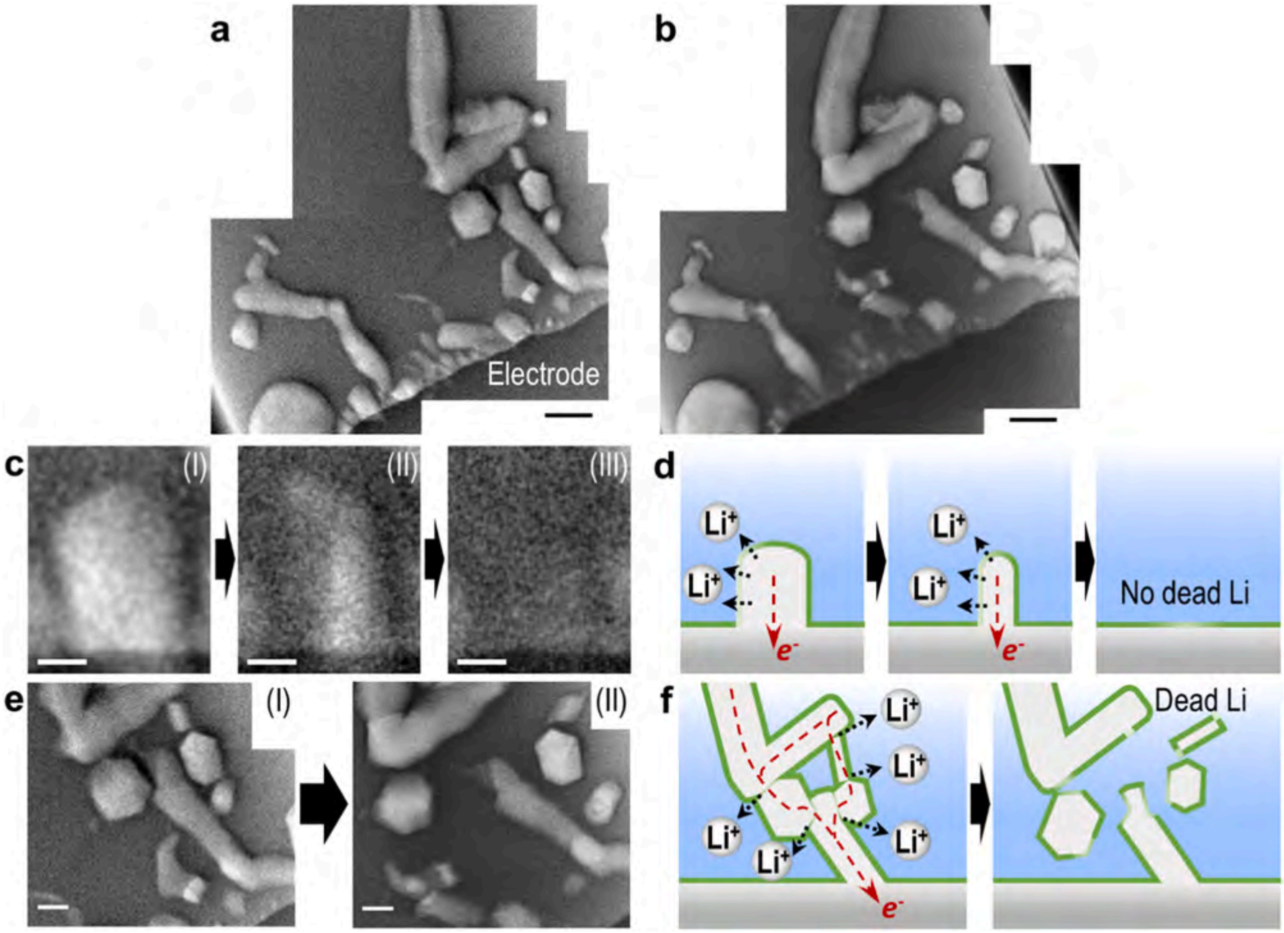

Fig. 5. Stripping modes of lithium dendrites. (a, b) TEM images captured (a) during *in-situ* lithium plating and (b) after *in-situ* lithium stripping (Video S6). (c, e) Sequential TEM images of stripping and (d, f) corresponding schematic illustrations of lithium stripping modes: (c, d) surface-preferred (Video S7) and (e, f) interface-preferred asymmetric stripping modes. Scale bars: (a, b) 1 μm, (c) 200 nm, (e) 500 nm.

carefully designed to induce large and flat lithium growth for minimizing SEI areas while suppressing dendrite formation. It furthermore will reduce the interface-preferred lithium stripping and the severe SEI fragmentation, both of which will be beneficial to the Coulombic efficiency. In this regard, rigid artificial SEIs or host structures, which transform the lithium growth behavior [29–31], would also be helpful to seize SEIs during lithium stripping and encourage their functionality in the next cycle.

3. Conclusion

In conclusion, we revealed the stripping mechanisms of lithium deposits at the nanoscale by *in-situ* liquid cell TEM. It was found that lithium deposits are sporadically stripped and the stripping of individual lithium deposits can be described by one of the three modes regardless of their morphology as follows: (i) symmetric stripping, (ii) surface-preferred asymmetric stripping, and (iii) interface-preferred asymmetric stripping. Importantly, we found that the interface-preferred asymmetric stripping greatly contributes to the formation of dead lithium from typical lithium dendrites, which has not been fully understood so far. Furthermore, chemical analysis of SEI with exceptional spatial resolution unveiled that SEI fragments would float in the electrolyte rather than stably adhere to the electrode after lithium stripping. It suggests the necessity of rigid protection layers on the electrode to avoid wasting the “good SEI” formed in the prior cycle. This study provides a comprehensive understanding of the stripping behavior of lithium deposits, which is critical for the development of lithium metal batteries.

4.Material and methods

4.1. In-situ electrochemical liquid cell TEM experiments

Details of the titanium electrode-deposited liquid TEM cell fabrication and the Sn@SnO2 nanostructure-assisted PDDA cationic polymer synthesis and coating methods are described in our previous papers [11, 32,33]. Lithium flakes were attached onto both Ti electrodes to construct Li/Li symmetric cell. Liquid electrolyte (1 M lithium hexafluorophosphate ($LiPF_6$) solution in propylene carbonate (PC)) was loaded dropwise into the cell by a pipette. UV-curing adhesives were used to seal the liquid TEM cell reservoirs, which was fully cured within 30 s by a UV flashlight. The liquid TEM cell sample was prepared in an argon-filled glove box. The prepared liquid TEM cell was loaded into our customized *in-situ* TEM holder with electric cables extended to the tip of the holder. Protruding electric wires from the liquid TEM cell were bonded to the cables at the tip of the holder by silver conducting paste to establish electrical connection between the liquid TEM cell and an external potentiostat (CH Instruments). For the *in-situ* TEM lithium stripping experiments, lithium metal was pre-deposited in the liquid TEM cell in the TEM column by voltammetry method (a linear sweep potential from 0 to −4 V at 0.1 V/s sweep rate, followed by a constant potential bias of −4 V), as shown in our previous paper.[11] A positive potential was applied (a linear sweep potential from 0 to +4 V at 0.1 V/s sweep rate, followed by a constant potential bias of +4 V) to the liquid

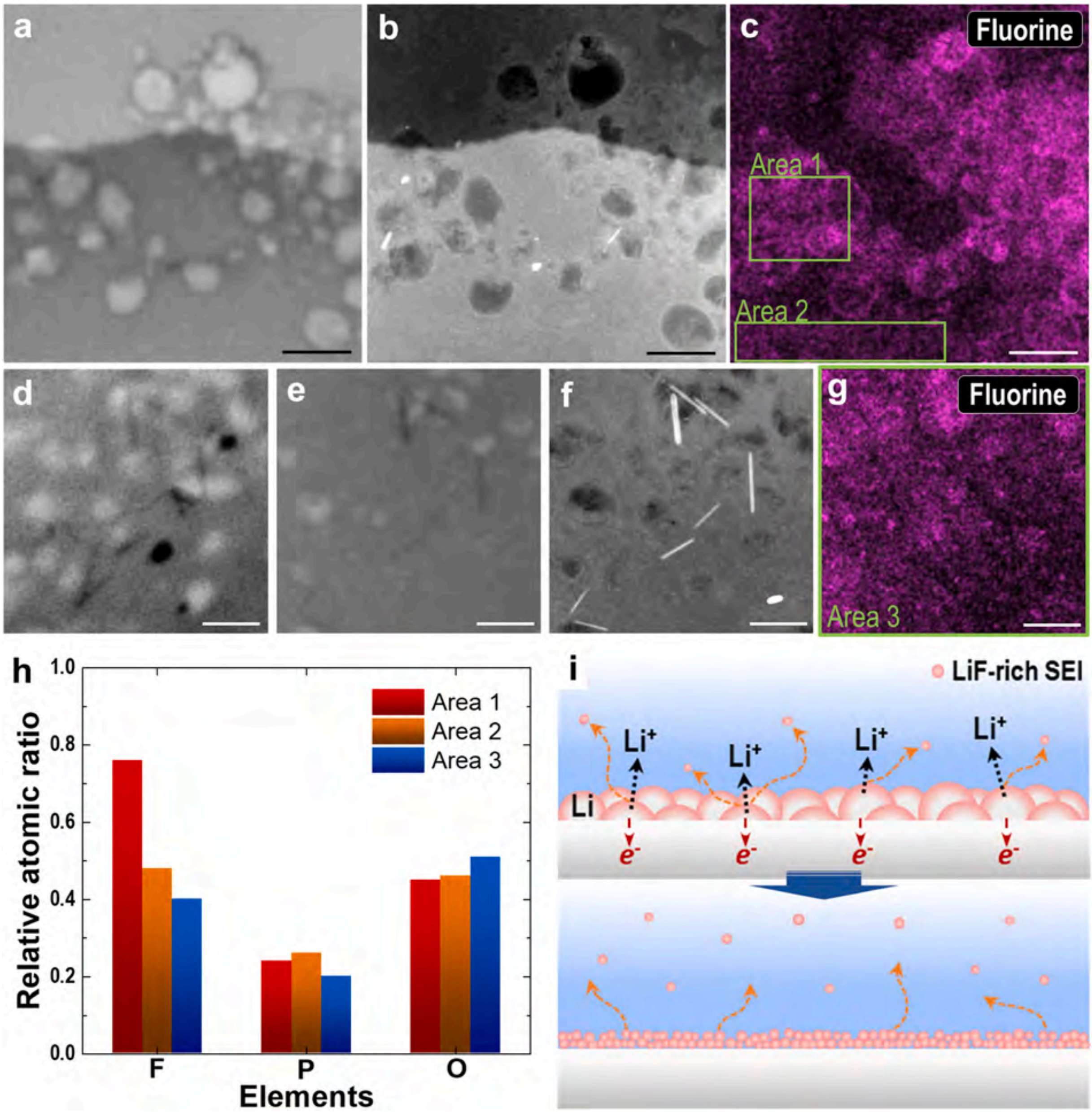

Fig. 6. A comparison of SEI layers before and after the lithium stripping. (a) A TEM image, (b) a corresponding ADF-STEM image, and (c) a corresponding EDS fluorine map of *in-situ* plated lithium nanogranules with LiF-rich SEI. Lower half area with different contrasts in the TEM/STEM images corresponds to Ti electrode. (d, e) TEM images of the electrode area captured (d) before and (e) after *in-situ* lithium stripping. The images are a top view of a portion of the Ti electrode. (f) An ADF-STEM image and (g) an EDS fluorine map of *in-situ* lithium stripped area corresponding to (e). Bright objects in the STEM image are assistant nanorods used for the polymer film coating. All scale bars are 500 nm. (h) Atomic ratios of fluorine (n_F/n_{Ti}), phosphorus (n_P/n_{Ti}), and oxygen (n_O/n_{Ti}) relative to titanium electrode at selected areas marked in (c) and (g), calculated from the EDS results. (i) Schematic illustration of stripping behaviors of lithium deposits and their SEI layers.

TEM cells in the TEM column for the following *in-situ* TEM lithium stripping experiments. Voltage and current profiles are shown in Figure S8 in Supplementary Material. The reactions were recorded at two frames per second (2 fps) by a charge-coupled device (CCD) camera installed in the TEM. Electron beam with very low electron dose rate of ~0.2–0.5 $e^-/Å^2s$ was used during the lithium stripping experiments to avoid unexpected effects by the electron beam. For STEM-EDS measurements, post-mortem analysis was performed after opening the liquid TEM cell to acquire high EDS signal. Before opening the liquid cell, liquid electrolyte was solidified on the *in-situ* grown lithium deposits to make a protection layer. The detailed procedure is described as follows. Electron beam with a low but slightly higher electron dose rate of ~1 $e^-/Å^2s$ was used to irradiate the *in-situ* experimented liquid TEM cell for more than 20 min, to polymerize (solidify) the liquid electrolyte.[34] The polymerized electrolyte acts as a protection layer for the underlying lithium deposits and electrodes. Before the STEM-EDS measurements, the top and bottom chips of the liquid TEM cell were carefully separated to obtain more EDS signals. Both sides (top and bottom) of SiN window membranes remained on the bottom liquid TEM cell, which covered the top and bottom sides of the lithium deposits making double protection layers together with the polymerized electrolyte layer. These layers protected the lithium deposits and the electrodes from air exposure before the cell loading into the TEM column. The *in-situ* liquid cell TEM experiments were performed with JEOL JEM-2100 200 kV LaB_6 TEM instrument and the STEM-EDS experiments were performed with FEI Themis 300 kV field-emission TEM instrument equipped with Bruker SuperX EDS detectors.

4.2. Video/image noise reduction

Some videos and images were processed for noise reduction. For Video S1 (Figs. 2a, b, 4a, and 6 d), four consecutive frames were averaged to reduce random noise. Subsequently, outliers were removed by replacing each pixel with the median of the surrounding two-pixel radius if it deviates from the median by more than 20 (raw unit). Same procedure was performed for Video S2-S5 (Fig. 2d, e, g, i), except two consecutive frames were averaged to reduce random noise. In addition, total variation denoising (also known as ROF denoising) was performed with the regularization parameter $\lambda = 0$ [35]. All noise reduction process was performed using Fiji (ImageJ) software.

CRediT authorship contribution statement

Seung-Yong Lee: Conceptualization, Methodology, Investigation, Formal analysis, Writing – original draft. **Junyi Shangguan**: Methodology, Resources. **Sophia Betzler**: Methodology, Resources. **Stephen J. Harris**: Writing – review & editing. **Marca M. Doeff**: Writing – review & editing. **Haimei Zheng**: Conceptualization, Methodology, Writing – review and editing, Supervision.

Declaration of Competing Interest

The authors do not have conflict-of-interest.

Data Availability

Data will be made available on request.

Acknowledgements

This work was supported by the U.S. Department of Energy (DOE), Office of Science, Basic Energy Sciences (BES), Materials Sciences and Engineering Division under Contract No. DE-AC02-05-CH11231 within the KC22ZH program. Part of S.Y.L.'s effort was supported by National Research Foundation of Korea (NRF) grant funded by the Korea government(MSIT) (No. NRF-2021R1F1A1051412 and NRF-2022R1C1C1010157), and the research fund of Hanyang University (HY-202100000000761). Work at the Molecular Foundry (TMF)of Lawrence Berkeley National Laboratory (LBNL) was supported by the Office of Science, Office of Basic Energy Sciences, of the U.S. Department of Energy under Contract No. DE-AC02–05CH11231. STEM-EDS experiments were conducted using ThemIS TEM instrument at National Center for Electron Microscopy (NCEM) of TMF at LBNL. S.J.H. was supported by the Assistant Secretary for Energy Efficiency, Vehicle Technologies Office of the U.S. Department of Energy under the Advanced Battery Materials Research Program. We thank Dr. Karen Bustillo, Dr. Rohan Dhall, Dr. Chengyu Song, Dr. Stefano Cabrini, Dr. Selven Virasawmy at LBNL for their generous help on setting up the experiments. We also thank Prof. Wenhao Sun at University of Michigan for useful discussions.

Appendix A. Supporting information

Supplementary data associated with this article can be found in the online version at doi:10.1016/j.nanoen.2022.107641.

References

[1] D.C. Lin, Y.Y. Liu, Y. Cui, Reviving the lithium metal anode for high-energy batteries, Nat. Nanotechnol. 12 (2017) 194–206.
[2] Y.P. Guo, H.Q. Li, T.Y. Zhai, Reviving lithium-metal anodes for next-generation high-energy batteries, Adv. Mater. 29 (2017).
[3] L.L. Li, S.Y. Li, Y.Y. Lu, Suppression of dendritic lithium growth in lithium metal-based batteries, Chem. Commun. 54 (2018) 6648–6661.
[4] C.C. Fang, J.X. Li, M.H. Zhang, Y.H. Zhang, F. Yang, J.Z. Lee, M.H. Lee, J. Alvarado, M.A. Schroeder, Y.Y.C. Yang, B.Y. Lu, N. Williams, M. Ceja, L. Yang, M. Cai, J. Gu, K. Xu, X.F. Wang, Y.S. Meng, Quantifying inactive lithium in lithium metal batteries, Nature 572 (2019) 511 (+).
[5] K.H. Chen, K.N. Wood, E. Kazyak, W.S. LePage, A.L. Davis, A.J. Sanchez, N. P. Dasgupta, Dead lithium: mass transport effects on voltage, capacity, and failure of lithium metal anodes, J. Mater. Chem. A 5 (2017) 11671–11681.
[6] C.B. Jin, T.F. Liu, O.W. Sheng, M. Li, T.C. Liu, Y.F. Yuan, J.W. Nai, Z.J. Ju, W. K. Zhang, Y.J. Liu, Y. Wang, Z. Lin, J. Lu, X.Y. Tao, Rejuvenating dead lithium supply in lithium metal anodes by iodine redox, Nat. Energy 6 (2021) 378–387.
[7] F. Wu, Y.X. Yuan, X.B. Cheng, Y. Bai, Y. Li, C. Wu, Q. Zhang, Perspectives for restraining harsh lithium dendrite growth: towards robust lithium metal anodes, Energy Stroage Mater. 15 (2018) 148–170.
[8] K.J. Harry, D.T. Hallinan, D.Y. Parkinson, A.A. MacDowell, N.P. Balsara, Detection of subsurface structures underneath dendrites formed on cycled lithium metal electrodes, Nat. Mater. 13 (2014) 69–73.
[9] Y.Z. Li, Y.B. Li, A.L. Pei, K. Yan, Y.M. Sun, C.L. Wu, L.M. Joubert, R. Chin, A.L. Koh, Y. Yu, J. Perrino, B. Butz, S. Chu, Y. Cui, Atomic structure of sensitive battery materials and Interfaces revealed by cryo-electron microscopy, Science 358 (2017) 506–510.
[10] M.J. Zachman, Z.Y. Tu, S. Choudhury, L.A. Archer, L.F. Kourkoutis, Cryo-STEM mapping of solid-liquid interfaces and dendrites in lithium-metal batteries, Nature 560 (2018) 345.
[11] S.-Y. Lee, J. Shangguan, J. Alvarado, S. Betzler, S.J. Harris, M.M. Doeff, H. Zheng, Unveiling the mechanisms of lithium dendrite suppression by cationic polymer film induced solid-electrolyte interphase modification, Energy Environ. Sci. 13 (2020) 1832–1842, https://doi.org/10.1039/d0ee00518e.
[12] X.B. Cheng, R. Zhang, C.Z. Zhao, F. Wei, J.G. Zhang, Q. Zhang, A review of solid electrolyte interphases on lithium metal anode, Adv. Sci. 3 (2016).
[13] N.J. Dudney, Approaches toward lithium metal stabilization, MRS Bull. 43 (2018) 752–758.
[14] Y. Gao, Z.F. Yan, J.L. Gray, X. He, D.W. Wang, T.H. Chen, Q.Q. Huang, Y.G.C. Li, H. Y. Wang, S.H. Kim, T.E. Mallouk, D.H. Wang, Polymer-inorganic solid-electrolyte interphase for stable lithium metal batteries under lean electrolyte conditions, Nat. Mater. 18 (2019) 384.
[15] F.N. Jiang, S.J. Yang, H. Liu, X.B. Cheng, L. Liu, R. Xiang, Q. Zhang, S. Kaskel, J. Q. Huang, Mechanism understanding for stripping electrochemistry of Li metal anode, SusMat 1 (2021) 506–536.
[16] F.F. Shi, A. Pei, D.T. Boyle, J. Xie, X.Y. Yu, X.K. Zhang, Y. Cui, Lithium metal stripping beneath the solid electrolyte interphase, P Natl. Acad. Sci. USA 115 (2018) 8529–8534.
[17] H. Liu, X.B. Cheng, R. Xu, X.Q. Zhang, C. Yan, J.Q. Huang, Q. Zhang, Plating/Stripping behavior of actual lithium metal anode, Adv. Energy Mater. 9 (2019), https://doi.org/10.1002/aenm.201902254.
[18] J. Kasemchainan, S. Zekoll, D.S. Jolly, Z.Y. Ning, G.O. Hartley, J. Marrow, P. G. Bruce, Critical stripping current leads to dendrite formation on plating in lithium anode solid electrolyte cells, Nat. Mater. 18 (2019) 1105.
[19] J. Steiger, D. Kramer, R. Monig, Mechanisms of dendritic growth investigated by in situ light microscopy during electrodeposition and dissolution of lithium, J. Power Sources 261 (2014) 112–119.
[20] G. Yoon, S. Moon, G. Ceder, K. Kang, Deposition and stripping behavior of lithium metal in electrochemical system: continuum mechanics study, Chem. Mater. 30 (2018) 6769–6776.
[21] D. Tewari, P.P. Mukherjee, Mechanistic understanding of electrochemical plating and stripping of metal electrodes, J. Mater. Chem. A 7 (2019) 4668–4688.
[22] N. Hodnik, G. Dehm, K.J.J. Mayrhofer, Importance and challenges of electrochemical in situ liquid cell electron microscopy for energy conversion, Res. Acc. Chem. Res. 49 (2016) 2015–2022.
[23] Z.Y. Zeng, X.W. Zhang, K. Bustillo, K.Y. Niu, C. Gammer, J. Xu, H.M. Zheng, In situ study of lithiation and delithiation of MoS2 nanosheets using electrochemical liquid cell transmission electron microscopy, Nano Lett. 15 (2015) 5214–5220.
[24] X.L. Fan, L. Chen, X. Ji, T. Deng, S.Y. Hou, J. Chen, J. Zheng, F. Wang, J.J. Jiang, K. Xu, C.S. Wang, Highly fluorinated interphases enable high-voltage Li-metal, Batter., Chem. -Us 4 (2018) 174–185.
[25] S. Choudhury, L.A. Archer, Lithium fluoride additives for stable cycling of lithium batteries at high current densities, Adv. Electron Mater. 2 (2016).
[26] S.J. Pennycook, Structure determination through Z-contrast microscopy, Adv. Imaging Electron Phys. Vol 123 (123) (2002) 173–206.
[27] R.E. PATTLE, DIFFUSION FROM AN INSTANTANEOUS POINT SOURCE WITH A CONCENTRATION-DEPENDENT COEFFICIENT, Q. J. Mech. Appl. Math. 12 (1959) 407–409, https://doi.org/10.1093/qjmam/12.4.407.
[28] X.L. Fan, X. Ji, F.D. Han, J. Yue, J. Chen, L. Chen, T. Deng, J.J. Jiang, C.S. Wang, Fluorinated solid electrolyte interphase enables highly reversible solid-state Li metal battery, Sci. Adv. 4 (2018).
[29] B. Zhu, Y. Jin, X.Z. Hu, Q.H. Zheng, S. Zhang, Q.J. Wang, J. Zhu, Poly (dimethylsiloxane) thin film as a stable interfacial layer for high-performance lithium-metal battery anodes, Adv. Mater. 29 (2017).
[30] D.C. Lin, Y.Y. Liu, Z. Liang, H.W. Lee, J. Sun, H.T. Wang, K. Yan, J. Xie, Y. Cui, Layered reduced graphene oxide with nanoscale interlayer gaps as a stable host for lithium metal anodes, Nat. Nanotechnol. 11 (2016) 626.
[31] G.Y. Zheng, S.W. Lee, Z. Liang, H.W. Lee, K. Yan, H.B. Yao, H.T. Wang, W.Y. Li, S. Chu, Y. Cui, Interconnected hollow carbon nanospheres for stable lithium metal anodes, Nat. Nanotechnol. 9 (2014) 618–623.
[32] Z.Y. Zeng, W.I. Liang, H.G. Liao, H.L.L. Xin, Y.H. Chu, H.M. Zheng, Visualization of electrode-electrolyte interfaces in LiPF6/EC/DEC electrolyte for lithium ion batteries via in Situ TEM, Nano Lett. 14 (2014) 1745–1750.

[33] M.H. Sun, H.G. Liao, K.Y. Niu, H.M. Zheng, Structural and morphological evolution of lead dendrites during electrochemical migration, Sci. Rep. -Uk 3 (2013).
[34] I.A. Shkrob, Y. Zhu, T.W. Marin, D. Abraham, Reduction of carbonate electrolytes and the formation of Solid-Electrolyte Interface (SEI) in lithium-ion batteries. 2. radiolytically induced polymerization of ethylene carbonate, J. Phys. Chem. C. 117 (2013) 19270–19279.
[35] L.I. Rudin, S. Osher, E. Fatemi, Nonlinear total variation based noise removal algorithms, Phys. D. 60 (1992) 259–268.